Journal of Power Sources 243 (2013) 891–898

Contents lists available at SciVerse ScienceDirect

Journal of Power Sources

journal homepage: www.elsevier.com/locate/jpowsour

# Improving the electrochemical performance of anatase titanium dioxide by vanadium doping as an anode material for lithium-ion batteries

Ly Tuan Anh [1], Alok Kumar Rai [1], Trang Vu Thi, Jihyeon Gim, Sungjin Kim, Eui-Chol Shin, Jong-Sook Lee, Jaekook Kim*

*Department of Materials Science and Engineering, Chonnam National University, 300 Yongbong-dong, Bukgu, Gwangju 500-757, Republic of Korea*

## HIGHLIGHTS

- A study on $V^{5+}$ doped $TiO_2$ as a high performance anode for lithium ion battery.
- $V^{5+}$ doping significantly influence the crystal structure and particle sizes.
- The electronic conductivity is largely improved through $V^{5+}$ doping.
- $V^{5+}$ doping greatly increased both the reversible capacity and cycling stability of $TiO_2$.

## ARTICLE INFO

*Article history:*
Received 27 March 2013
Received in revised form
12 June 2013
Accepted 14 June 2013
Available online 22 June 2013

*Keywords:*
Titanium dioxide
Vanadium
Semiconductor
Anode
Lithium ion battery

## ABSTRACT

Undoped and 2 wt% vanadium ($V^{5+}$) doped $TiO_2$ samples are prepared in polyol medium by low-temperature solvothermal method. The as-prepared samples are annealed at 400 °C for 5 h in an air atmosphere to increase the crystallinity. The XRD pattern shows that pure anatase $TiO_2$ is formed in both the doped and undoped samples. The maximum sizes of nanoparticles are found to be 300 nm and 15 nm with spherical shaped morphology for undoped $TiO_2$ and $V^{5+}$ doped $TiO_2$ samples respectively. In addition, 2 wt% $V^{5+}$ doped sample exhibits excellent electrochemical performance with high reversible specific capacity and excellent rate capability compared to the undoped case. This improvement can be attributed to the substitution of the $Ti^{4+}$ ions by $V^{5+}$ ions in the $TiO_2$ lattice and create more $Ti^{4+}$ vacancies in the lattice. This action may lead to the generation of apparently more number of free holes in the doped p-type semiconductor. Therefore, the increased hole concentration in the valence band can contribute to the electrical conductivity of the doped sample. Vanadium doping also influences the sample crystallinity and reduces the particle size, which provides a larger active surface area than that of undoped $TiO_2$.



## 1. Introduction

Lithium-ion batteries (LIBs) are widely used in portable devices such as mobile phones, laptops, and cameras. They have also been considered as important power sources for Electric Vehicles (EV), Hybrid Electric Vehicles (HEV), Plug-in Hybrid Electric Vehicles (PHEV), and other electric utilities due to the properties related to lightness, compactness, working voltage, and energy density [1]. However, LIBs in such applications call for high safety standards and low-cost materials. Furthermore, increased environmental problems have also prompted the development of green processes for LIB production and disposal [2]. Therefore, many studies have been performed to find appropriate electrode materials. Currently, titanium dioxide ($TiO_2$) is one of the most attractive anode materials for LIBs due to its high capability, long cycle life, high safety, low cost, nontoxicity, and the fact that it is environmentally benign. $TiO_2$ has three common polymorphs: anatase, rutile, and brookite. They offer structurally non-equivalent host lattices for the insertion of Li ions in $Li_xTiO_2$ [3]. The lithium insertion coefficient $x$ ($Li_xTiO_2$) may depend on the crystallography and structure of particular materials. The most active form of $TiO_2$ for Li ion insertion and extraction is the anatase phase, which has a reversible insertion coefficient of up to over 0.5 mol lithium per mol of $TiO_2$ at room

* Corresponding author. Tel.: +82 62 530 1703; fax: +82 62 530 1699.
*E-mail address:* jaekook@chonnam.ac.kr (J. Kim).
[1] These authors contributed equally to this work.

0378-7753/$ – see front matter © 2013 Elsevier B.V. All rights reserved.
http://dx.doi.org/10.1016/j.jpowsour.2013.06.080

temperature [4]. In contrast, only a small amount of lithium can be inserted into rutile and brookite $TiO_2$ at room temperature [3]. Thus, anatase $TiO_2$ has been one of the best candidates for the anode material of LIBs. As an anode, the operating voltage of $TiO_2$ ($\sim$1.7 V vs. $Li^+$/Li) is higher than those of anode materials based on carbon ($\sim$0.1 V vs. $Li^+$/Li) [5,6]. Although the high operating voltage of $TiO_2$ reduces the overall cell voltage, it will prevent the formation of a Solid Electrolyte Interface (SEI) layer under 1 V, which can lead to irreversible capacity and obstruct the movement of lithium ions. Inhibiting the formation of a SEI layer may improve the kinetic properties during lithiation and delithiation. However, the poor electrical conductivity and low diffusion coefficient of $Li^+$ ions in this material has restricted the application of $TiO_2$ as an anode material for LIBs [7]. Many efforts have been made to improve the electrical conductivity and diffusion coefficient of $Li^+$ ions in $TiO_2$ structure. To increase the diffusion coefficient, attempts have been made to shorten the $Li^+$ ion diffusion distance in the bulk material by using nanomaterials such as nanoparticles [8], nanotubes [9], nanowires [10], and nanoporous structures [11]. In addition, many studies have been conducted to improve the electron transport in $TiO_2$ materials by making nanocomposites with graphene [12], using conductive coatings (carbon [13], Ag [4] and Sn [14]) as well as other methods. In addition, $TiO_2$ is a semiconducting metal oxide with semiconductor properties. The electrical conductivity of $TiO_2$ depends on the free electrons or holes concentration contributed by oxygen vacancies or interstitial metal atoms in the material. Therefore, in the reported literature, to increase the free electron concentration in the conduction band and thus improve the electrical conductivity, $TiO_2$ has been doped with higher-valence elements such as Vanadium ($V^{5+}$), Niobium ($Nb^{5+}$), and Tantalum ($Ta^{5+}$) [15–17].

In this paper, we investigate the electrochemical performances of optimized $V^{5+}$ doping in $TiO_2$ as a negative electrode for LIBs, which has never been reported to the best of our knowledge. The superior electrochemical performances of doped samples in comparison to undoped samples clearly shows the $V^{5+}$ doping effect, which increased the electrical conductivity, diffusion coefficient, kinetic properties during lithiation and delithiation and additional electrochemical active sites to further enhance their electrochemical performance.

## 2. Experiment

### 2.1. Material synthesis

Vanadium ($V^{5+}$) doped $TiO_2$ sample was prepared in polyol medium by low-cost solvothermal method [18] using titanium (IV) tetraisopropoxide (TTIP) {$Ti[OCH(CH_3)_2]_4$, 98%, Junsei Chemicals, Japan} and vanadium (V) oxytriisopropoxide (VOTP) {$C_9H_{21}O_4V$, 98%, Sigma–Aldrich, USA} as precursor materials. Diethylene Glycol (DEG) {$C_4H_{10}O_3$, 99%, Dae-Jung Chemicals, South Korea} was used as a solvent. TTIP was first dissolved into 15 ml of DEG and stirred for 2 h. An appropriate calculated amount of VOTP (with the optimal value of atomic ratio V/Ti of 0.02 or 2 wt%) was added and stirred for 5 h to obtain a suspension. The resulting solution was sealed in a 40-ml Teflon-line bomb and placed into a drying oven pre-heated at 235 °C, where it was kept at that temperature for 16 h. After cooling and ultrasonication, the resulting precipitates were washed with acetone and methanol several times to remove residual organic constituents before filtering using ceramic membrane funnels and drying in a vacuum chamber for 12 h at 120 °C. The obtained sample was thoroughly ground using an agate mortar and annealed at 400 °C for 5 h to increase the crystallinity of the sample. The undoped $TiO_2$ sample was synthesized and annealed under the same conditions without the addition of VOTP for comparison.

### 2.2. Structure and morphology characterization

The crystal structure of undoped and $V^{5+}$ doped $TiO_2$ samples were characterized by X-ray diffraction (XRD, Shimadzu X-ray diffractometer) using Cu K$\alpha$ radiation ($\lambda$ = 1.5406 Å). The surface morphology and particles sizes were analyzed by field-emission scanning electron microscopy (FE-SEM, S-4700 Hitachi) and field-emission transmission electron microscopy (FE-TEM, Philips Tecnai F20 at 200 kV). The samples were soaked in ethanol and dispersed by ultrasonic vibration before coating onto copper grids for FE-TEM examination. The annealed sample of $V^{5+}$ doped $TiO_2$ was examined by X-ray photoelectron spectroscopy (XPS) using a Thermo VG Scientific instrument, Multilab 2000 in order to establish the valence states of Ti and V respectively. XPS measurements were carried out using a dual anode X-ray source Al K$\alpha$ radiation ($h\nu$ = 1486.6 eV). The spectrometer was calibrated with respect to the C1s peak (binding energy 285 eV).

### 2.3. Electrochemical measurement

The working electrodes were fabricated by mixing the active material (80 wt%) with super-P (10 wt%) and polyvinylidene fluoride (10 wt%) in *N*-methyl-2-pyrrolidone to form a slurry. The resulting slurry was coated onto a copper foil current collector and dried under vacuum at 80 °C overnight. The slurry was punched into circular electrodes after pressing between stainless steel twin rollers, in order to improve the contact between the active material and copper foil. The electrolyte used was 1 M $LiPF_6$ dissolved in a mixture of ethylene carbonate (EC) and dimethylcarbonate (DMC) (1:1 in volume ratio). The 2032 coin-type cells were assembled in a glove box under a dry argon atmosphere using lithium metal as a reference electrode, and a polymer membrane together with glass fiber as a separator. Coin cells were kept in the glove box for 12 h for aging before electrochemical measurements. Galvanostatic testing (BTS–2004H, Nagano, Japan) was used to investigate the electrochemical performance over the potential range of 1.0–3.0 V vs. $Li^+$/Li at different current densities.

The electrical characterization of the bulk samples were performed on both undoped $TiO_2$ and $V^{5+}$ doped $TiO_2$ pellets (9 Φ diameter) prepared from about 160 mg of powder, similarly as done for dense sintered reduced $TiO_2$ samples [19]. The cold isostatically pressed pellets were heat-treated at 350 °C for 6 h for mechanical stability. Impedance was measured by a frequency response analyzer (Novocontrol GmbH, Germany) on the samples with indium electrodes applied by soldering. In addition an electrochemical C–V profiling of the $TiO_2$|electrolyte interface was performed in a home-made electrochemical test station using a potentiostat/galvanostat/EIS analyzer (Autolab, Metrohm B.V. The Netherlands) with an Ag/AgCl reference electrode. An indium electrode was applied as an ohmic back contact. The electrolyte was a NaOH solution of pH = 13.

## 3. Results and discussion

### 3.1. Crystal structure and morphology

Fig. 1(a and b) shows the XRD patterns of as-prepared and annealed samples of undoped and 2 wt% $V^{5+}$ doped $TiO_2$, respectively. All peaks were exactly matched to pure $TiO_2$ with tetragonal anatase phase (JCPDS card no. 89-4921, space group: $I4_1/amd(141)$). No impurities could be detected in the XRD patterns. It is reasonable to suggest that the $V^{5+}$ ions might substitute the $Ti^{4+}$ ions in the $TiO_2$ lattice due to its small ionic radius (0.53 Å) than that of $Ti^{4+}$ ions (0.68 Å). It can be clearly observed that the crystallinity of as-prepared sample of undoped $TiO_2$ is quite low, and has structure

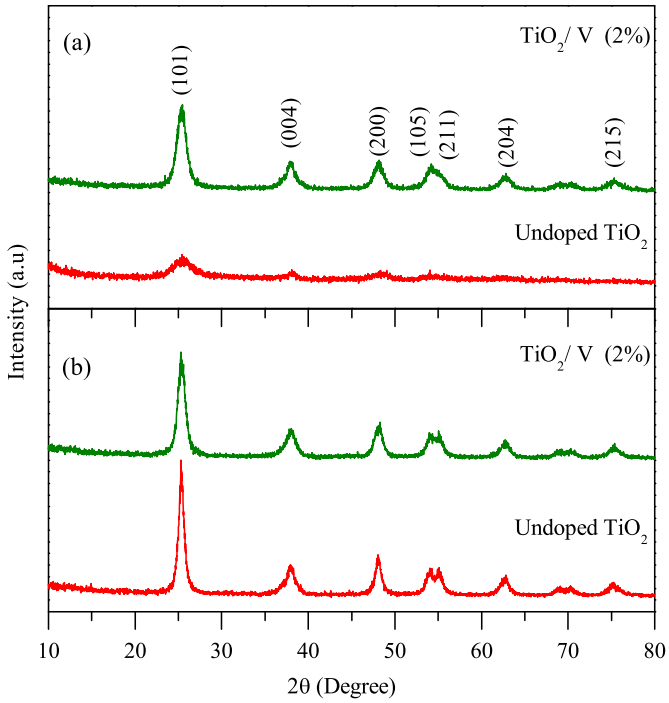


**Fig. 1.** X-ray diffraction patterns of undoped and $V^{5+}$ doped $TiO_2$ samples: (a) As-prepared and (b) annealed samples at 400 °C for 5 h.

similar to amorphous (non-crystalline) structure (Fig. 1(a)). In contrast, the amount of crystallinity is increased due to the effect of $V^{5+}$ doping during the synthesis, as presented in Fig. 1(a).

The FE-SEM analysis was used to examine the surface morphology of the obtained samples and presented in Fig. 2. The FE-SEM images of the as-prepared and annealed samples of undoped $TiO_2$ show a large spherical particles distribution, as shown in Fig. 2(a and b). In fact, the larger particles with agglomerated nanostructure participate in a conversion mechanism that could be detrimental to electrochemical performances [18]. However, the $V^{5+}$ doped $TiO_2$ samples exhibit distinct differences in surface morphology and particle sizes due to the influence of doping in both the as-prepared and annealed samples compared to the undoped sample, as can be observed in Fig. 2(c and d). The doped samples had small spherical particles, which were agglomerated due to their extremely small dimensions and high surface energy. In addition, the dependency of particle-size properties on temperature for the prepared samples can be more clearly understood on a combined analysis of the XRD and SEM results in Figs. 1 and 2 respectively. A careful observation of Fig. 1(a) and Fig. 2(a, b) leads one to conclude that the sample crystallinity and density increases while particles sizes seem to decrease significantly after heat treatment of the undoped $TiO_2$ sample at 400 °C. The reason for the shrinkage in particle-sizes due to heat treatment may be attributed to the evaporation of absorbed water and organic impurities in the as-prepared sample. On the other hand, the comparison of Fig. 1(b) and Fig. 2(c, d) indicate that, although, improvement in sample crystallinity occurs no significant variation is observed in particle-size after annealing the doped sample. However, the annealing of the doped sample improves the cyclability and C-rate performance, as observed from the results of the electrochemical measurements (Figs. 5, 6 and 10) discussed later. Overall, it can be concluded that vanadium-doping indeed facilitates the production of highly crystalline samples.

In order to further investigate the effect of $V^{5+}$ doping on the $TiO_2$ morphology, FE-TEM was also carried out, as shown in Fig. 3. Fig. 3(a and b) shows the large particle sizes of the undoped samples which are as large as 300 nm for both the as-prepared and annealed sample. However, the maximum average particles size for

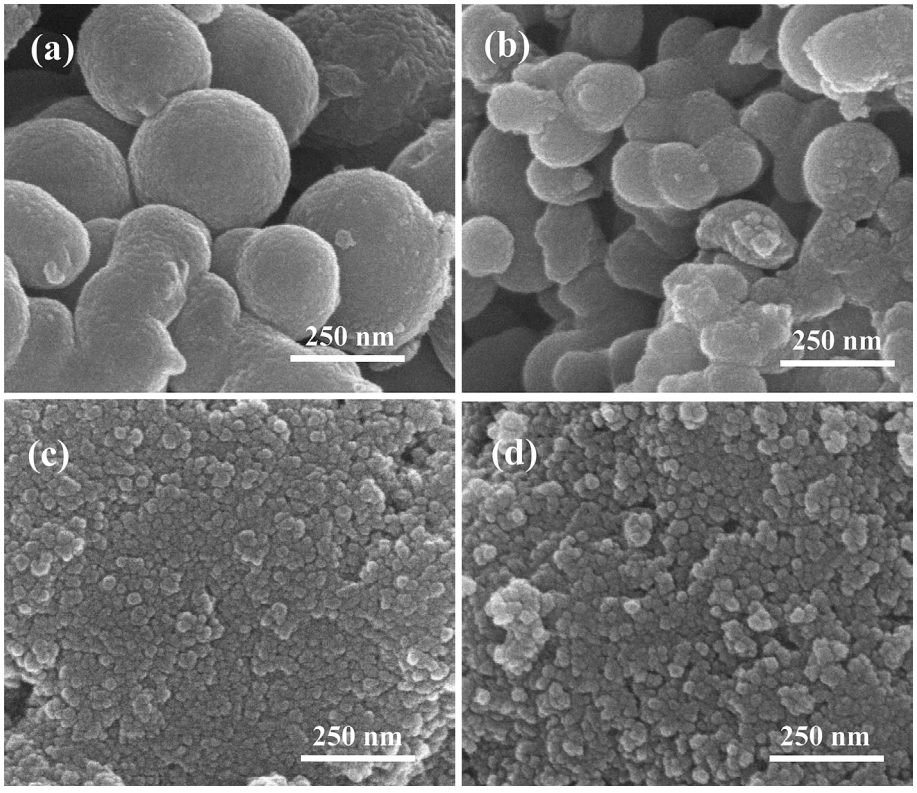


**Fig. 2.** FE-SEM images: (a) as-prepared and (b) annealed sample of undoped $TiO_2$; (c) as-prepared and (d) annealed sample of $V^{5+}$ doped $TiO_2$.

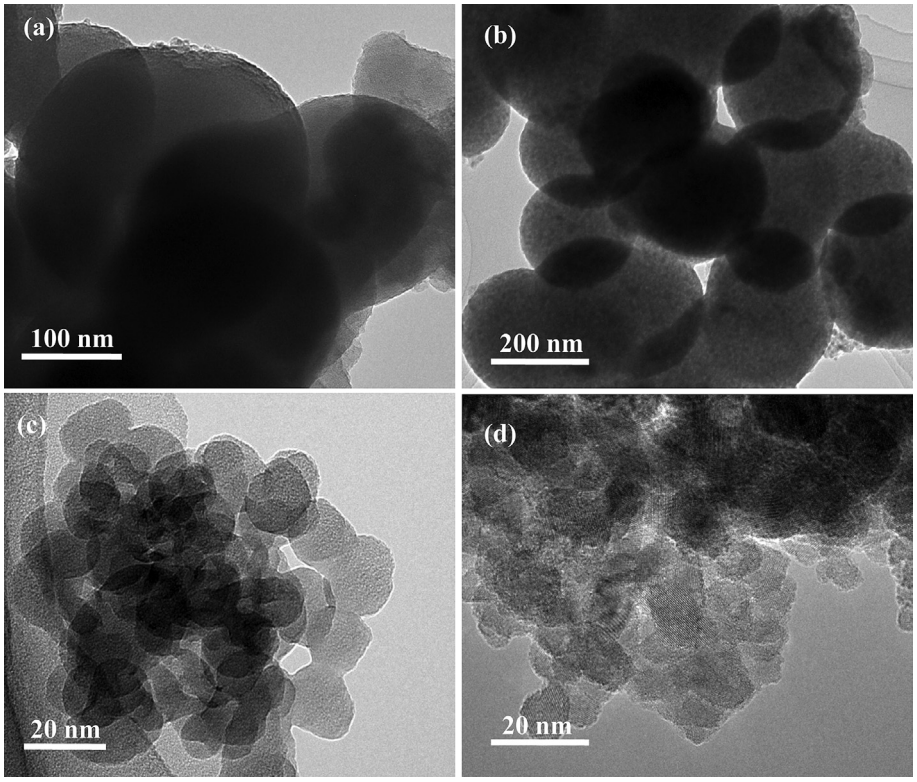


**Fig. 3.** FE-TEM images: (a) as-prepared and (b) annealed sample of undoped $TiO_2$; (c) as-prepared and (d) annealed sample of $V^{5+}$ doped $TiO_2$.

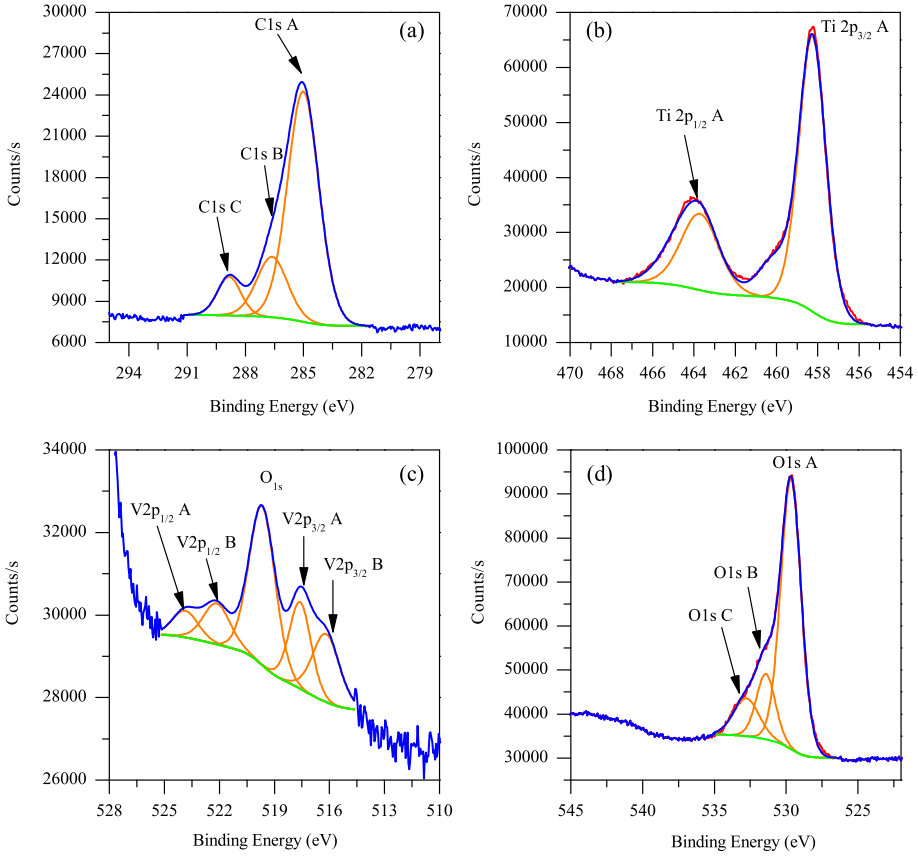


**Fig. 4.** XPS patterns of C1s (a); Ti2p (b); V2p (c); and O1s (d) in $V^{5+}$ doped $TiO_2$ powder heat treated under air atmosphere.

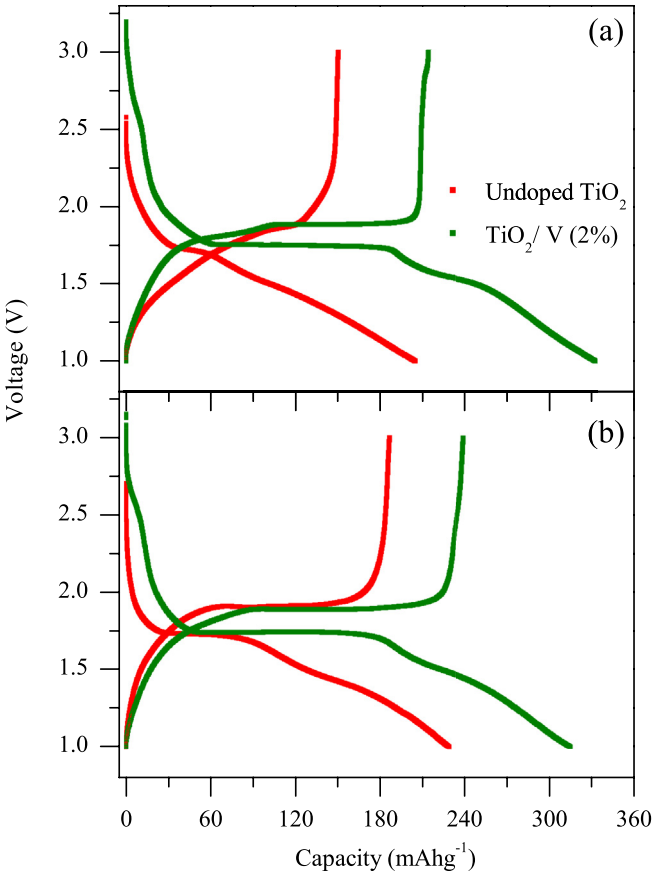


**Fig. 5.** Initial charge/discharge profiles of undoped and $V^{5+}$ doped $TiO_2$ electrodes: (a) As-prepared and (b) annealed samples.

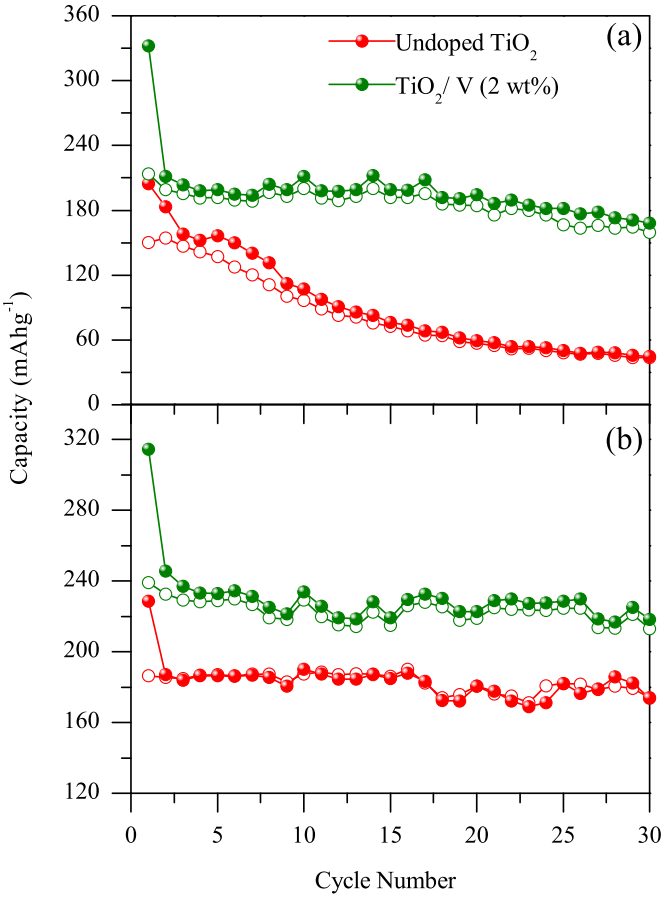


**Fig. 6.** Cycling performances of undoped and $V^{5+}$ doped $TiO_2$ electrodes: (a) as-prepared and (b) annealed samples.

the $V^{5+}$ doped samples is 15 nm, which are much smaller than those of the undoped cases, as presented in Fig. 3(c and d). These differences clearly indicated the role and influence of $V^{5+}$ doping into the structure of $TiO_2$. In addition, the smaller nanoparticles allowed quicker lithium-ion intercalation and deintercalation due to the short distances for lithium-ion transport within the particles.

The present solvothermal preparation route is believed to facilitate a substitution of the $V^{5+}$ ion for the $Ti^{4+}$ ions in $TiO_2$ lattice, which was further confirmed by XPS analysis. XPS is a useful technique extensively used to evaluate the valence states of chemical elements in nanomaterials synthesized by various strategies. Obvious C1s, Ti2p, V2p and O1s peaks were detected, and the high-resolution spectra of all these elements are shown in Fig. 4(a–d), respectively. As shown in Fig. 4(a), the C1s spectrum of $V^{5+}$ doped $TiO_2$ sample presents three small typical peaks at 285.2 eV (A), 286.6 eV (B) and 288.8 eV (C), which can be assigned to C–C, C–O and O–C=O groups, respectively [20]. In Fig. 4(b), the Ti2P peaks that located around 458.2 and 463.7 eV are the Ti 2p3/2 (A) peak and Ti 2p1/2 (A) peak, respectively, demonstrating the existence and occupying of $Ti^{4+}$ in an octahedral environment. In addition, the peak separation of 5.5 eV in the obtained binding energies also offers good agreement with literature value [15,21]. Fig. 4(c) shows the highly resolved V2p XPS peak and its fitted Gaussian peaks. As can be seen from figure, the binding energy of V are located at 517.6 and 523.8 eV for 2p3/2 (A) and 2p1/2 (A) splits, respectively, and the difference is around 6.2 eV, matching well with the binding energies of $V^{5+}$ ions [15]. In addition, we also observe a weak intensity peaks at around 516.1 and 522.2 eV for 2p3/2 (B) and 2p1/2 (B), which represents the +4 oxidation state of V [15,22]. The peak at 520 eV is due to the O1s satellite peak, which indicates the hybridization between V-3d and O-2p levels. Fig. 4(d) showed the XPS spectra of the O1s region. Generally, the photoelectron peaks of O1s could be resolved into three components. The dominant peak at about 529.7 eV (A) was characteristic of metallic oxides, which was in agreement with O1s electron binding energy arising from vanadium and titanium lattices. The O1s peak at 531.4 eV (B) and 532.8 eV (C) was respectively corresponding to the surface hydroxyl and adsorbed oxygen mainly from adsorbed water molecules [15].

### 3.2. Electrochemical performance

Fig. 5(a and b) shows the initial charge/discharge voltage profiles of as-prepared and annealed samples of undoped and 2 wt% $V^{5+}$ doped $TiO_2$, respectively at a constant current density of 0.1 mA $cm^{-2}$ between the potential range of 1.0–3.0 V vs. $Li^+$/Li. As expected, in both the case, the $V^{5+}$ doped samples clearly display the plateaus in their respective ~1.75 V and ~1.88 V regions for discharging and charging, respectively, which are exactly similar to previously reported literature of anatase $TiO_2$ [8,23,24]. In addition, it can be also observed that the as-prepared sample of undoped $TiO_2$ (Fig. 5a) shows a comparatively short plateau probably due to its insufficient crystalline character [3]. In the first discharge process, the potential rapidly drops and reaches a plateau of ~1.75 V, and then gradually decreases to 1.0 V. A short voltage plateau near 1.55 V can also be observed within the sloped region from ~1.75 to 1.0 V. Firstly, within the region between the initial OCV and ~1.75 V

a rather sloping voltage profile corresponds to a solid solution insertion mechanism, indicating to an initial lithium insertion in the anatase $TiO_2$ host structure. The main flat voltage plateau is characteristic of a two-phase electrochemical reaction [25,26], and the lithium insertion proceeds through a two-phase equilibrium of a Li-poor (space group *I41/amd*) and a Li-rich phase (space group *Imma*) [25,27]. After this main voltage plateau the potential drops again, and at ~1.55 V a second plateau is observed, corresponding to the second phase transition from Li-rich titanate to a second anatase phase ($Li_1TiO_2$, space group *I41/amd*) [28]. The wide potential plateaus also indicate that the insertion and extraction of lithium ions occur in one stage [25,29]. In addition, the particular voltage plateaus at ~1.75 V and ~1.88 V of the doped samples also become larger than those of the undoped samples, which clearly revealed the influence of $V^{5+}$ doping in enhancing the energy storage capability of anatase $TiO_2$ when used as anode materials for LIBs. The irreversible capacity loss was observed during the first cycle that is expected for most anodes due to the surface reaction between the electrode and electrolyte, and the incomplete extraction of intercalated $Li^+$ ions upon deintercalation [30]. As presented in Fig. 5(a), the charge capacity of $V^{5+}$ doped as-prepared sample was 213.9 mAh $g^{-1}$ and that of the annealed sample was 239.0 mAh $g^{-1}$ in the first cycle, as shown in Fig. 5(b). These values were 63.7 mAh $g^{-1}$ and 52.6 mAh $g^{-1}$ higher than that of undoped samples, which are 150.2 mAh $g^{-1}$ and 186.4 mAh $g^{-1}$, respectively. More importantly, the voltage profiles of the $V^{5+}$ doped $TiO_2$ nanoparticles electrodes display smaller polarization ($V_{ch} - V_{dis}$) than that of the undoped $TiO_2$ nanoparticles electrodes is due to the more electronically conducting $V^{5+}$ doped samples. Moreover, the $V^{5+}$ doped (2 wt%) $TiO_2$ electrodes show more capacity compared to that of undoped $TiO_2$ nanoparticles electrodes, which can be attributed to the large electrochemical active surface-area of doped samples, reduced resistance and more grain boundary areas of the $TiO_2$ nanoparticles in the doped samples.

Another advantage of the $V^{5+}$ doped $TiO_2$ electrodes is significantly improved cycling performance compared with undoped $TiO_2$ nanoparticles electrodes. Fig. 6 shows the cycling behavior of the undoped and $V^{5+}$ doped $TiO_2$ nanoparticles electrodes at a constant current density of 0.1 mA $cm^{-2}$. After charging and discharging for 30 cycles, the as-prepared sample of $V^{5+}$ doped $TiO_2$ showed good capacity retention (159.3 mAh $g^{-1}$ of charge capacity in the 30th cycle), which was much better than that of the value of 43.5 mAh $g^{-1}$ for the undoped $TiO_2$ electrode, as shown in Fig. 6(a). In the case of the annealed samples (Fig. 6(b)), both the doped and undoped electrodes indicated very good cycling performances with clear differences between their specific capacities over 30 cycles. Both undoped and $V^{5+}$ doped $TiO_2$ electrodes exhibit second reversible charge capacities are 185.5 mAh $g^{-1}$ and 232.6 mAh $g^{-1}$, respectively and could retain almost 174.1 mAh $g^{-1}$ and 213.1 mAh $g^{-1}$, respectively after 30 cycles, which are equivalent to 93% and 92% of the second reversible capacity, demonstrating excellent capacity retention of the annealed electrodes (Fig. 6(b)). The enhanced capacities as a result of the $V^{5+}$ doping increase the diffusion rate of $Li^+$ ions into the $TiO_2$ structure, less nanometer sizes of particles provides larger active surface area and high degree of crystallization reduces the number of lattice defects, which facilitates the lithium ions insertion and extraction processes. In addition, the capacity enhancement can also be attributed to the substitution of the $Ti^{4+}$ ions by $V^{5+}$ ions in the $TiO_2$ lattice and create more $Ti^{4+}$ vacancies ($V_{Ti}''''$) in the lattice, as can be demonstrated in Fig. 7. Titanium vacancies are native defects in $TiO_2$ [31] responsible p-type insulating behavior of undoped $TiO_2$ as shown by Mott–Schottky behavior shown in Fig. 8, which is in contrast to the n-type behavior of the reduced $TiO_2$ [19]. The overall impedance behavior of In|$TiO_2$|NaOH cell was very complex and time-dependent due to the high resistance and the porosity. The capacitance at 10 kHz from the initial bias seep was used for the analysis. $Ti^{4+}$ vacancies ($V_{Ti}''''$) generated by $V^{5+}$ doping provide higher acceptor centers which is indicated by the increased dopant density in V–$TiO_2$ in Fig. 8. The hole concentration was estimated as $1.75 \times 10^{10}/cm^{-3}$ and $9.28 \times 10^{11}/cm^{-3}$, respectively using the nominal electrolyte/semiconductor contact area. Due to the uncertainty in the effective contact area, the estimates can be considered only for comparative purpose. The flat band potential of undoped $TiO_2$ estimated as 3 V vs. Ag/AgCl reference electrode is consistent with valence band edge of p-type $TiO_2$ as also shown for p-type $Fe_2O_3$ [32]. The flat band potential of 0.4 V for V–$TiO_2$ seems not to be straightforwardly explained.

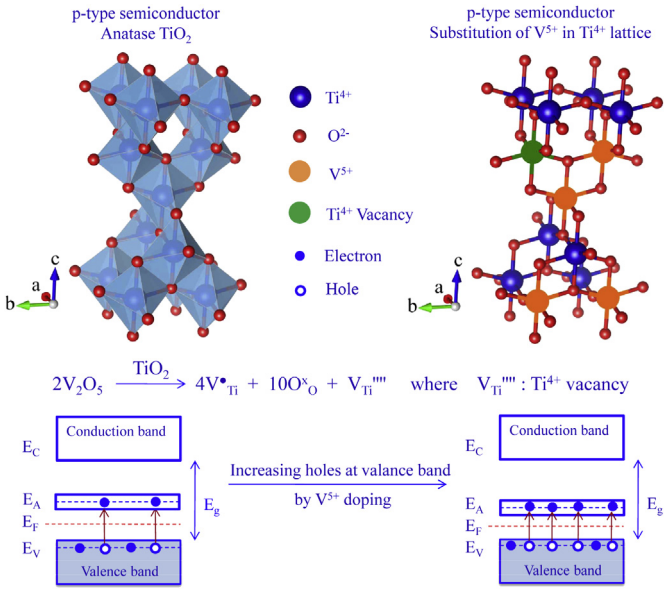


**Fig. 7.** Schematic illustration of $V^{5+}$ doped $TiO_2$ (p-type semiconductor) and demonstrating the increased electronic conductivity.

The conductivity enhancement due to the increased hole concentration is directly shown by the impedance measurements displayed in Fig. 9 using symmetric indium electrodes. The low frequency polarization indicates the ionic contribution in as-prepared rather insulating $TiO_2$ material, which should be

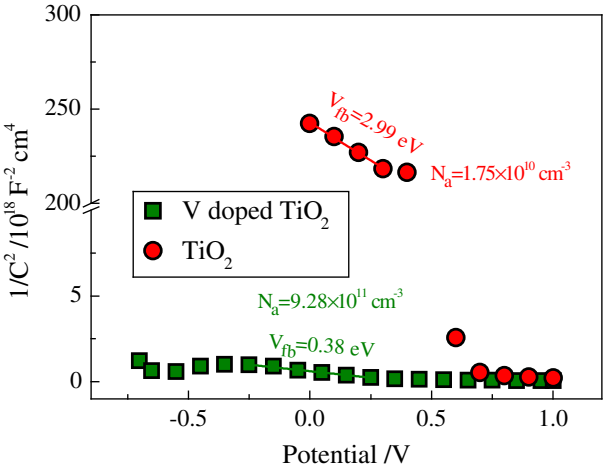


**Fig. 8.** Mott–Schottky plot of undoped and $V^{5+}$ doped $TiO_2$ electrodes using indium back contact in 0.1 M NaOH aqueous solution with reference to Ag/AgCl electrodes.

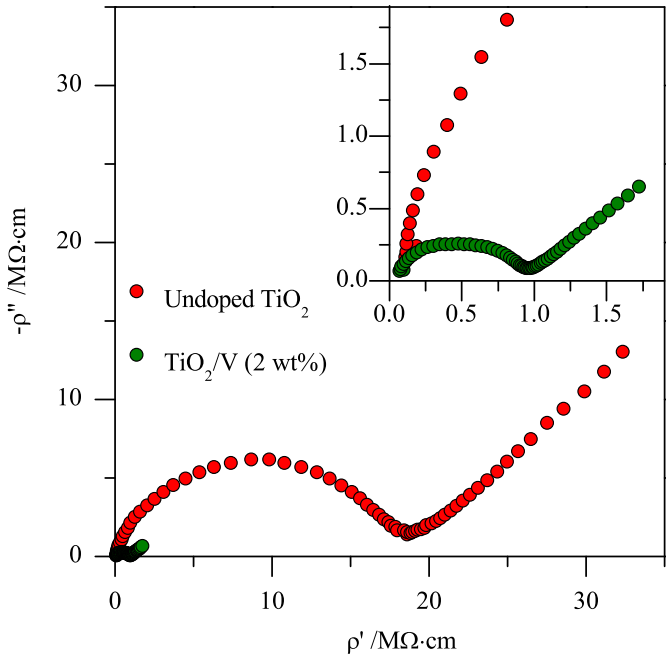


**Fig. 9.** Impedance spectra of undoped and $V^{5+}$ doped $TiO_2$ pellets with indium symmetric electrodes at room temperature.

attributed to oxide ions. The electronic conductivity of the $V^{5+}$ doped $TiO_2$ sample was approximately $1.15 \times 10^{-6}\ \Omega^{-1}\ cm^{-1}$. In comparison to the result of the undoped $TiO_2$ nanoparticles (electronic conductivity $5.61 \times 10^{-8}\ \Omega^{-1}\ cm^{-1}$), the conductivity of $V^{5+}$ doped $TiO_2$ nanoparticles with 2 wt% V content is almost 20 times higher, as shown in Fig. 8. Therefore, it can be concluded that the higher electronic conductivity would enable the $V^{5+}$ doped $TiO_2$ sample to present a better electrochemical capability, especially rate capability.

To examine the effectiveness of $V^{5+}$ doping in improving the rate capability of anode, we investigated the specific capacity of undoped $TiO_2$ nanoparticles and $V^{5+}$ doped $TiO_2$ nanoparticles electrodes under various current densities and the results are plotted in Fig. 10. Both the cells were cycled between 1.0 and 3.0 V under various current densities from 0.1 mA $cm^{-2}$ to 10 mA $cm^{-2}$. In the case of as-prepared samples (Fig. 10(a)), the specific capacity of the undoped $TiO_2$ nanoparticles electrode approached only ~7 mAh $g^{-1}$ when the current density was 10 mA $cm^{-2}$. The value was higher for the $V^{5+}$ doped electrode, at ~40 mAh $g^{-1}$. The $V^{5+}$ doped as-prepared sample showed clear improvement of rate capability at the other current densities also. This difference became larger and could be observed more clearly with increasing current density for the case of annealed samples in Fig. 10(b). The $V^{5+}$ doped annealed electrode delivers an initial charge capacity 239.0 mAh $g^{-1}$ at 0.1 mA $cm^{-2}$, 211.5 mAh $g^{-1}$ at 0.2 mA $cm^{-2}$, 213.7 mAh $g^{-1}$ at 0.4 mA $cm^{-2}$, 203.1 mAh $g^{-1}$ at 0.8 mA $cm^{-2}$, 189.2 mAh $g^{-1}$ at 1.6 mA $cm^{-2}$, 173.7 mAh $g^{-1}$ at 3.2 mA $cm^{-2}$, 153.0 mAh $g^{-1}$ at 6.4 mA $cm^{-2}$ and 136.5 mAh $g^{-1}$ at 10 mA $cm^{-2}$. While the undoped electrode exhibit an initial charge capacity of 186.4 mAh $g^{-1}$, 176.9 mAh $g^{-1}$, 160.2 mAh $g^{-1}$, 134.4 mAh $g^{-1}$, 109.0 mAh $g^{-1}$, 83.4 mAh $g^{-1}$, 59.0 mAh $g^{-1}$ and 44.4 mAh $g^{-1}$ at the same current densities. More importantly, when the testing current returned to a lower current rate of 0.1 mA $cm^{-2}$, the charge/discharge capacities recovered to the same levels initially shown at that rate. Since $Li^+$ ion diffusion is dependent on the ion-transport length and accessible active material surface sites, the $V^{5+}$ doped

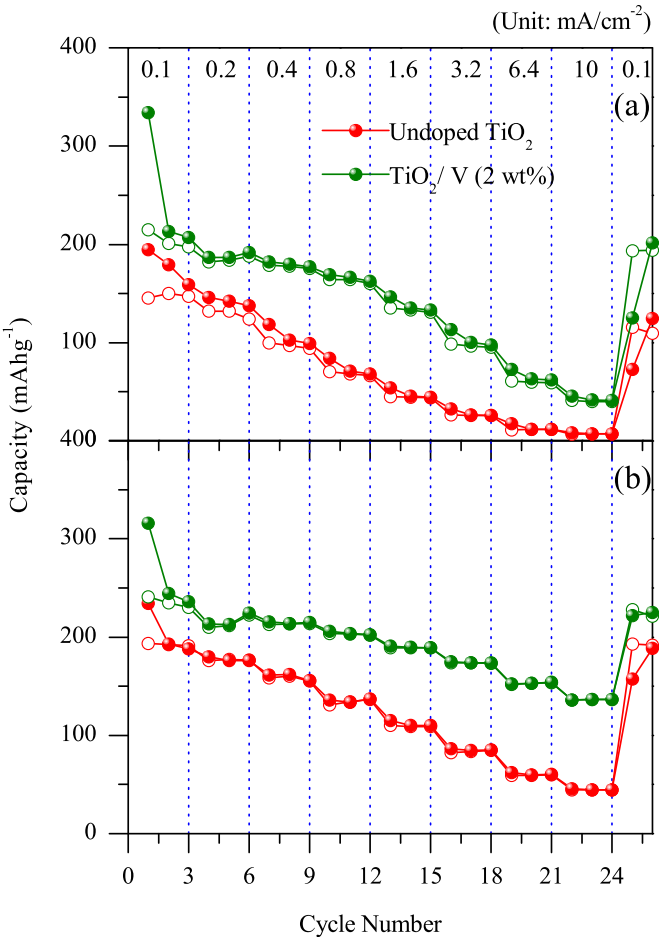


**Fig. 10.** Comparison of the rate capabilities of undoped and $V^{5+}$ doped $TiO_2$ electrodes: (a) As-prepared and (b) annealed samples.

nanosized $TiO_2$ particles may provide shorter ion transport path lengths and enhancements in electrode/electrolyte contact area and thereby lead to higher storage capacities, coulombic efficiencies and cycling stabilities. Further, a combined analysis of the XRD, FE-SEM and electrochemical measurement results of the doped samples suggest that, although, not much variation in particle-sizes are observed between the as-prepared and annealed samples, the apparently higher crystalline characteristics may significantly contribute to the better electrochemical performance in the annealed sample.

## 4. Conclusion

Undoped and 2 wt% $V^{5+}$ doped $TiO_2$ samples are successfully synthesized using a cost-effective precursor and a low-temperature solvothermal method in polyol medium. The XRD patterns indicate that a single phase of anatase $TiO_2$ is formed, and no phase changes occurred after annealing at 400 °C for 5 h. The maximum sizes of nanoparticles are found to be 300 nm and 15 nm with spherical shaped morphology for undoped $TiO_2$ and $V^{5+}$ doped $TiO_2$ samples respectively. When tested for lithium storage, the optimized 2 wt% $V^{5+}$ doped $TiO_2$ electrodes demonstrate significantly improved cycling performance and rate capability compared to the undoped $TiO_2$ nanoparticles electrode. Moreover, the annealed sample of $V^{5+}$ doped $TiO_2$ electrode exhibits a second reversible charge capacity of 232.6 mAh $g^{-1}$ at 0.1 mA $cm^{-2}$ and more importantly, could retain almost 213.1 mAh $g^{-1}$ without obvious capacity fading over

30 cycles, demonstrating excellent capacity retention of the electrode. After 30 cycles, the capacity attain for the $V^{5+}$ doped sample is 23% higher than that observed for undoped $TiO_2$ nanoparticles electrode (174.1 mAh $g^{-1}$). Even at a high current density of 10 mA $cm^{-2}$, the reversible capacity of $V^{5+}$ doped annealed $TiO_2$ nanoparticles electrode is still as high as 136.5 mAh $g^{-1}$, which is higher than that of the undoped $TiO_2$ nanoparticles electrode (44.4 mAh $g^{-1}$). The improved electrochemical performances of $V^{5+}$ doped $TiO_2$ samples clearly indicates the distinct influence of doping, which increases the electrical conductivity, diffusion coefficient, kinetic properties during lithiation and delithiation and additional electrochemical active surface sites to further enhance their electrochemical performance. The obtained results reveal the potential of $V^{5+}$ doping to enhance the electrochemical performance of anatase $TiO_2$ used as an anode material for LIBs.

## Acknowledgments

This research was supported by World Class University (WCU) program through the Korea Science and Engineering Foundation funded by the Ministry of Education, Science and Technology (R32-20074). This work was also supported by Priority Research Centers Program through the National Research Foundation of Korea (NRF) funded by the Ministry of Education, Science and Technology (2009-0094055). We thank Mr. Dong-Chun Jo for the experimental assistance.

## References

[1] T.F. Yi, H. Liu, Y.R. Zhu, L.J. Jiang, Y. Xie, R.S. Zhu, J. Power Sources 215 (2012) 258–265.
[2] M. Mancini, F. Nobili, R. Tossici, M. Wohlfahrt-Mehrens, R. Marassi, J. Power Sources 196 (2011) 9665–9671.
[3] J.W. Kang, D.H. Kim, V. Mathew, J.S. Lim, J.H. Gim, J. Kim, J. Electrochem. Soc. 158 (2011) A59–A62.
[4] M.M. Rahman, J.Z. Wang, D. Wexler, Y.Y. Zhang, X.J. Li, S.L. Chou, H.K. Liu, J. Solid State Electrochem. 14 (2010) 571–578.
[5] D.V. Bavykin, J.M. Friedrich, F.C. Walsh, Adv. Mater. 18 (2006) 2807–2824.
[6] X.P. Gao, Y. Lan, H.Y. Zhu, J.W. Liu, Y.P. Ge, F. Wu, D.Y. Song, Electrochem. Solid-State Lett. 8 (2005) A26–A29.
[7] X. Su, Q.L. Wu, X. Zhan, J. Wu, S. Wei, Z. Guo, J. Mater. Sci. 47 (2012) 2519–2534.
[8] A.K. Rai, L.T. Anh, J. Gim, V. Mathew, J. Kang, B.J. Paul, J. Song, J. Kim, Electrochim. Acta 90 (2013) 112–118.
[9] G.F. Ortiz, I. Hanzu, T. Djenizian, P. Lavela, J.L. Tirdo, P. Knauth, Chem. Mater. 21 (2009) 63–67.
[10] J.M. Li, W. Wang, H.H. Zhou, J.J. Li, D.S. Xu, Chem. Commun. 47 (2011) 3439–3441.
[11] J. Wang, Y.K. Zhou, Y.Y. Hu, R.O. Hayre, Z.P. Shao, J. Phys. Chem. C 115 (2011) 2529–2536.
[12] H.C. Tao, L.Z. Fan, X. Yan, X. Qu, Electrochim. Acta 69 (2012) 328–333.
[13] S.J. Park, Y.J. Kim, H. Lee, J. Power Sources 196 (2011) 5133–5137.
[14] H.S. Kim, S.H. Kang, Y.H. Chung, Y.E. Sung, Electrochem. Solid-State Lett. 13 (2010) A15–A18.
[15] L. Li, C.Y. Liu, Y. Liu, Mater. Chem. Phys. 113 (2009) 551–557.
[16] Y. Liu, J.M. Szeifert, J.M. Feckl, B. Mandlmeier, J. Rathousky, O. Hayden, D. Fattakhova-Rohlfing, T. Bein, ACS Nano 4 (2010) 5373–5381.
[17] X. Feng, K. Shankar, M. Paulose, C.A. Grimes, Angew. Chem. Int. Ed. 48 (2009) 8095–8098.
[18] A.K. Rai, J. Gim, S.W. Kang, V. Mathew, L.T. Anh, J. Kang, J. Song, B.J. Paul, J. Kim, Mater. Chem. Phys. 136 (2012) 1044–1051.
[19] J. Moon, J.-A. Park, S.-J. Lee, J.-I. Lee, T. Zyung, E.-C. Shin, J.-S. Lee, Phys. Chem. Chem. Phys. 15 (2013) 9361–9374.
[20] Y.B. He, B. Li, M. Liu, C. Zhang, W. Lv, C. Yang, J. Li, H. Du, B. Zhang, Q.H. Yang, J.K. Kim, F. Kang, Sci. Rep. 2 (2012) 913.
[21] X. Lü, J. Li, X. Mou, J. Wu, S. Ding, F. Huang, Y. Wang, F. Xu, J. Alloys Compd. 499 (2010) 160–165.
[22] Y. Zhang, M. Fan, M. Zhou, C. Huang, C. Chen, Y. Cao, G. Xie, H. Li, X. Liu, Bull. Mater. Sci. 35 (2012) 369–376.
[23] A. Stashans, S. Lunell, R. Bergstrom, A. Hagfeldt, S.E. Lindquist, Phys. Rev. B 53 (1996) 159–170.
[24] S.W. Oh, S.H. Park, Y.K. Sun, J. Power Sources 161 (2006) 1314–1318.
[25] J. Xu, Y. Wang, Z. Li, W.F. Zhang, J. Power Sources 175 (2008) 903–908.
[26] A.N. Jansen, A.J. Kahaian, K.D. Kepler, P.A. Nelson, K. Amine, D.W. Dees, D.R. Vissers, M.M. Thackeray, J. Power Sources 81/82 (1999) 902–905.
[27] M.V. Koudriachova, N.M. Harrison, S.W. de Leeuw, Solid State Ionics 152/153 (2002) 189–194.
[28] A. Moretti, G.T. Kim, D. Bresser, K. Renger, E. Paillard, R. Marassi, M. Winter, S. Passerini, J. Power Sources 221 (2013) 419–426.
[29] B.L. He, B. Dong, H.L. Li, Electrochem. Commun. 9 (2007) 425–430.
[30] S. Brutti, V. Gentili, H. Menard, B. Scrosati, P.G. Bruce, Adv. Energy Mater. 2 (2012) 322–327.
[31] B.J. Morgan, G.W. Watson, Phys. Rev. B 80 (2009) 233102.
[32] J.E. Turner, M. Hendewerk, J. Parmeter, D. Neiman, G.A. Somorajai, J. Electrochem. Soc. 131 (1984) 1777–1783.